IOP Publishing Semiconductor Science and Technology
Semicond. Sci. Technol. 32 (2017) 095011 (9pp) https://doi.org/10.1088/1361-6641/aa7c58

Epitaxial growth of cobalt oxide phases on Ru(0001) for spintronic device applications

Opeyemi Olanipekun[1], Chad Ladewig[1], Jeffry A Kelber[1], Michael D Randle[2], Jubin Nathawat[2], Chun-Pui Kwan[2], Jonathan P Bird[2], Priyanka Chakraborti[3], Peter A Dowben[3], Tao Cheng[4] and W A Goddard III[4]

[1] Department of Chemistry, University of North Texas, Denton, TX 76203, United States of America
[2] Department of Electrical Engineering, University at Buffalo, the State University of New York, Buffalo, NY 14260-1900, United States of America
[3] Department of Physics and Astronomy, Nebraska Center for Nanostructures and Materials, University of Nebraska-Lincoln, Lincoln, NE 68588-0299, United States of America
[4] Materials and Process Simulation Center, California Institute of Technology, Pasadena, California 91125, United States of America

E-mail: kelber@unt.edu

Received 12 May 2017, revised 19 June 2017
Accepted for publication 28 June 2017
Published 17 August 2017

Abstract

Cobalt oxide films are of technological interest as magnetic substrates that may support the direct growth of graphene, for use in various spintronic applications. In this work, we demonstrate the controlled growth of both $Co_3O_4(111)$ and CoO(111) on Ru(0001) substrates. The growth is performed by Co molecular beam epitaxy, at a temperature of 500 K and in an O_2 partial pressure of 10^{-4} Torr for $Co_3O_4(111)$, and 7.5×10^{-7} Torr for CoO(111). The films are distinguished by their dissimilar Co 2p x-ray photoemission (XPS) spectra, while XPS-derived O/Co stoichiometric ratios are 1.33 for $Co_3O_4(111)$ and 1.1 for CoO(111). Electron energy loss (EELS) spectra for $Co_3O_4(111)$ indicate interband transitions at ~2.1 and 3.0 eV, while only a single interband transition near 2.0 eV is observed for CoO(111). Low energy electron diffraction (LEED) data for $Co_3O_4(111)$ indicate twinning during growth, in contrast to the LEED data for CoO(111). For $Co_3O_4(111)$ films of less than 20 Å average thickness, however, XPS, LEED and EELS data are similar to those of CoO(111). XPS data indicate that both Co oxide phases are hydroxylated at all thicknesses. The two phases are moreover found to be thermally stable to at least 900 K in UHV, while *ex situ* atomic force microscopy measurements of $Co_3O_4(111)$/Ru(0001) indicate an average surface roughness below 1 nm. Electrical measurements indicate that $Co_3O_4(111)$/Ru(0001) films exhibit dielectric breakdown at threshold voltages of ~1 MV cm^{-1}. Collectively, these data show that the growth procedures yield $Co_3O_4(111)$ films with topographical and electrical characteristics that are suitable for a variety of advanced device applications.

Supplementary material for this article is available online

Keywords: cobalt oxide, graphene, spintronics, magnetic oxides, molecular beam epitaxy

(Some figures may appear in colour only in the online journal)

1. Introduction

Cobalt oxide surfaces are of broad and long-standing interest in multiple areas of technology, ranging from catalysis [1, 2] and battery technology [3], to spintronic applications [4–6]. Recently, we have demonstrated the direct growth of graphene on nanoscale-thickness $Co_3O_4(111)$ films formed on Co(0001) [7]. This work revealed evidence of spin

polarization in the graphene domains [8], which was induced through its proximal contact to the magnetic oxide and which persisted to temperatures beyond 400 K. This discovery suggests a pathway to the realization of novel spintronic devices based on graphene, in which room temperature functionality is achieved without the need for problematic spin injection from magnetic contacts. Rather, spin polarization in such devices could instead be achieved *after* the carriers have been injected (from a nonmagnetic contact) into the graphene, simply by exploiting its proximity to the magnetic oxide. With the capacity existing to manipulate subsequent spin propagation via magnetic electrodes on the graphene surface, the realization of this polarization scheme has the potential to lead to new classes of low-power spintronic devices. Consequently, the growth of cobalt oxide films, along with relevant properties, such as their surface roughness and dielectric-breakdown strength, are of considerable interest.

Motivated by the above considerations, in this paper we focus on establishing the required conditions for cobalt oxide growth on Ru(0001), at film thicknesses well beyond 1 nm. Oxide growth on such surfaces may actually result in two different stoichiometric forms—Co_3O_4(111) and CoO(111)—with different electronic and magnetic properties. Consequently, it is important to understand the conditions under which these different forms are formed during synthesis, and to characterize them through detailed structural analyses. Specifically, due to the demonstrated capacity of Co_3O_4(111) to function as a platform for subsequent graphene synthesis [7, 8], in this work we focus on establishing the conditions necessary to ensure its growth, and on establishing how to distinguish this phase experimentally from CoO(111). Previous studies have reported on Co_3O_4(111) growth on Al_2O_3(0001) [9, 10], or on Ir(100) [11–13]. Ruthenium, however, is a material of general interest and exhibits compatibility with CMOS [14] and two-dimensional materials device applications [15]. It is thermally and chemically stable, and does not alloy with Co, thus making it suitable as a substrate for graphene/cobalt oxide applications. We also present here the first information on the surface roughness and dielectric-breakdown strength of the Co_3O_4(111) films. These spectroscopic and electrical data demonstrate the suitability of Co_3O_4 films for a variety of low-voltage, advanced device applications.

2. Experimental methods

Cobalt oxide film growth and *in situ* characterization were carried out in a vacuum system with three interconnected chambers, isolated by manual gate valves: (i) an introduction chamber connected to a turbo-molecular pump (base pressure: 10^{-8} Torr); (ii) a molecular beam epitaxy (MBE) chamber connected to a turbo-molecular pump (base pressure: 5×10^{-10} Torr), with capabilities for deposition and sample heating (300–1100 K) in reactive environments, and; (iii) an analysis chamber pumped with an ion/titanium sublimator pump (base pressure: 5×10^{-11} Torr). The analysis chamber is equipped with an unmonochromatized dual-anode x-ray source and double-pass cylindrical mirror analyzer with coaxial electron gun, permitting acquisition of x-ray photoemission spectroscopy (XPS), Auger electron spectroscopy (AES) and electron energy loss spectroscopy (EELS) data. The chamber is also equipped with a reverse-view low energy electron diffraction (LEED) I(V) system. The MBE chamber is equipped with a commercially available four-target electron beam evaporator. Sample transport between chambers was accomplished with a magnetically-coupled feedthrough. Pressures in all chambers were monitored with nude ion gauges, calibrated for N_2 and O_2 exposures, and were controlled with a manual leak valve using electronic-grade O_2.

The first step in the synthesis of the oxide films involved the growth of the ruthenium underlayer on an alumina substrate. In this step, Ru(0001) films were formed in a separate chamber by magnetron sputter deposition at 700 K in an Ar plasma (3.5 mTorr, 15 W), on commercially available (1 cm × 1 cm) Al_2O_3(0001). Prior to deposition, the substrates were cleaned by annealing them in O_2 (1000 K, 10^{-7} Torr). Deposited films exhibited typical sample roughness values of less than 1 nm and Ru thickness values of ∼500 Å or less, as determined by *ex situ* atomic-force microscopy (AFM) and x-ray reflectivity measurements (supplemental information, figure S1 is available online at stacks.iop.org/SST/32/095011/mmedia). Films were then transferred in air to the multichamber system for MBE and surface analysis. They were annealed in O_2 and in UHV at 1000 K to remove C and O, until they exhibited a sharp 1 × 1 LEED pattern. The presence of C was determined by measuring the ratio of the positive going peak to the negative-going AES peak near 273 eV, with a clean Ru surface exhibiting a ratio of ∼0.78 [16].

Once in the multichamber system, cobalt oxide films were grown at 500 K on the Ru(0001) substrates, by MBE performed with a Co-rod source at two different O_2 partial pressures; 10^{-4} Torr and 7.5×10^{-7} Torr. The average thickness of the resulting oxide film was determined as a function of Co deposition time by XPS measurements of the relative Co 2p and Ru 3d intensities [17], using a calculated Ru photoelectron inelastic mean free path length of 18.5 Å [18, 19]. This allowed measurements of films to thicknesses of ∼100 Å, beyond which point the Ru substrate 3d XPS signal was completely attenuated. Film thicknesses at longer growth times were therefore estimated by extrapolation of the growth rate derived for thinner films.

Various spectroscopic techniques were applied to the characterization of the synthesized films. XPS data were acquired with the double pass cylindrical mirror analyzer in constant pass energy mode, with Mg Kα radiation from the unmonochromatic dual anode source (operated at 15 kV and 300 W). EELS was performed in reflection mode at an electron beam energy of 100 eV, and analyses of the XPS and AES spectra were carried out by standard methods [17]. LEED data were analyzed using commercial software, which allowed a determination of the cobalt-oxide domain sizes [20]. AFM of the oxide films was performed in tapping mode using a Bruker Dimension Icon, capable of nanoscale surface

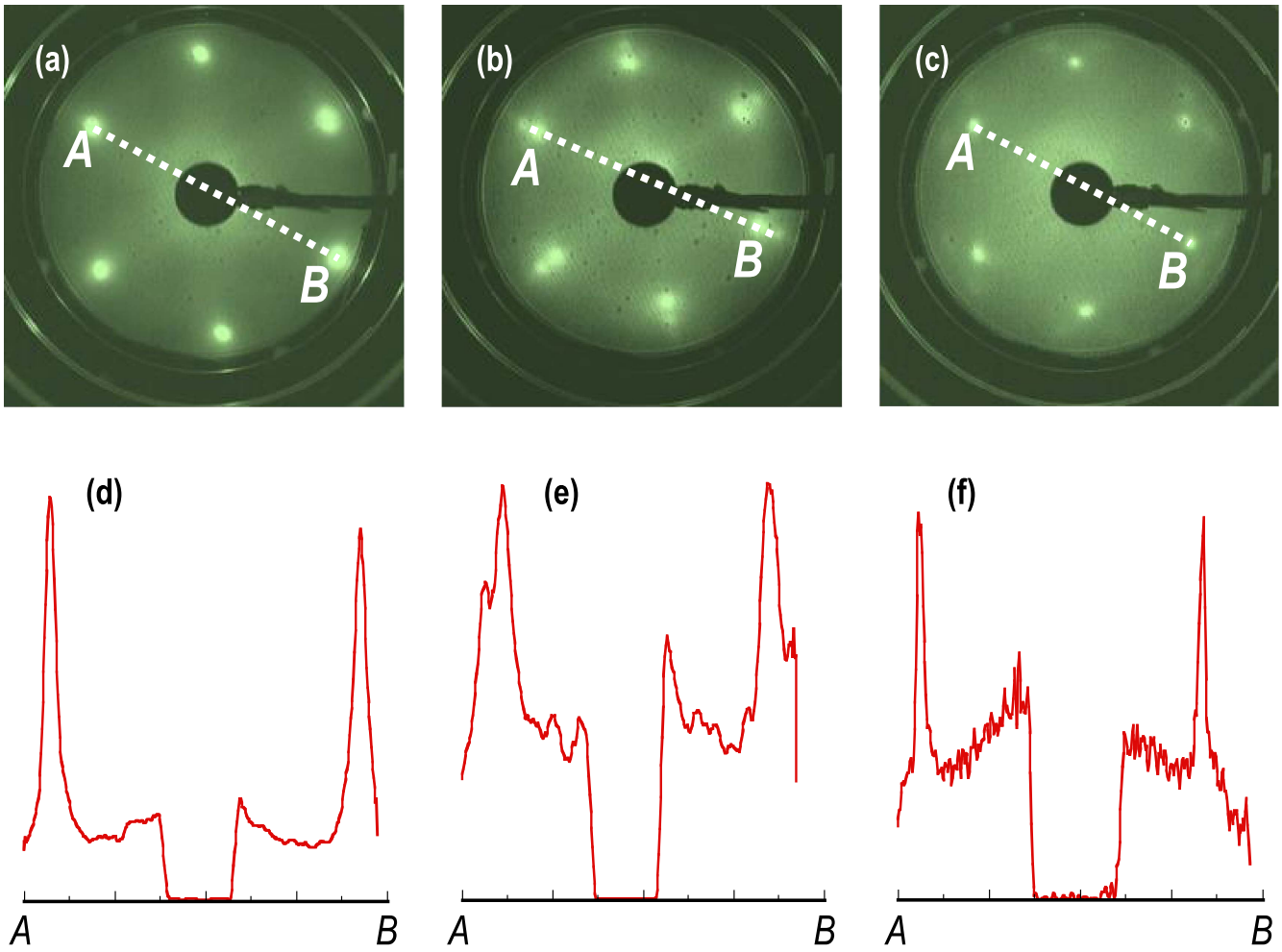

Figure 1. Evolution of the LEED spectra with CoO(111) film thickness. (a) Clean Ru(0001) substrate; (b) 20 Å thick CoO(111) film; (c) 370 Å thick Co(111) film. Corresponding linescan profiles are shown in panels (d)–(f), respectively. The oxide films were both grown at an oxygen pressure of 7.5×10^{-7} Torr at 500 K. All data were acquired at a beam energy of 60 eV.

topography and morphology measurements of a range of different surface types. Electrical breakdown of the films was explored in an ambient probe station.

3. Results

3.1. Cobalt oxide growth at low O_2 pressure: CoO(111) on Ru(0001)

In this section we discuss, first of all, our results for Co MBE in a low-pressure (7.5×10^{-7} Torr) O_2 environment, under which conditions we find that the growth results in the formation of CoO(111). The growth of Co_3O_4(111) in a high-pressure (10^{-4} Torr) O_2 environment is then discussed in the following section.

In figure 1 we present LEED data for a clean Ru(0001) film (see panel (a)) and for cobalt oxide films of two different thicknesses (20 and 370 Å, in panels (b) and (c), respectively). Corresponding LEED-spot linescan profiles are shown in figures 1(d)–(f), while XPS and EELS data are displayed in figure 2. The LEED data show that the resulting cobalt-oxide lattice is in azimuthal registry with that of the Ru(0001) substrate (as confirmed by the results of figure 1(b)), which show the Ru(0001) diffraction spots (outer circle) in registry with the CoO(111) diffraction spots (inner circle). Taking the Ru LEED data as indicating an in-plane lattice constant of 2.7 Å, we determine a lattice constant for the oxide of ∼3.0 Å, a value that is consistent with the formation of CoO(111) [13]. The diffraction spot size visibly decreases with increasing oxide thickness (see figures S2 and table S2), indicating that the average domain size of the oxide film increases as the growth proceeds. An analysis of the FWHM for a 370 Å thick film (figure 1(c)) indicates an average domain size of 27 (±2) nm.

Turning next to the results of our XPS measurements, the Co 2p spectra (figure 2(a)) did not change significantly with increasing film thickness, exhibiting main and satellite peaks that are characteristic of CoO [1, 21, 22]. An O 1s spectrum (figure 2(b), acquired for a film of 67 Å average thickness) remained unchanged over all film thicknesses examined, and indicated the existence of two O 1s chemical environments. The main peak, centered near 530.0 eV binding energy, is consistent with earlier reports for the binding energy of lattice oxygen in the oxide, while the higher-energy feature indicates

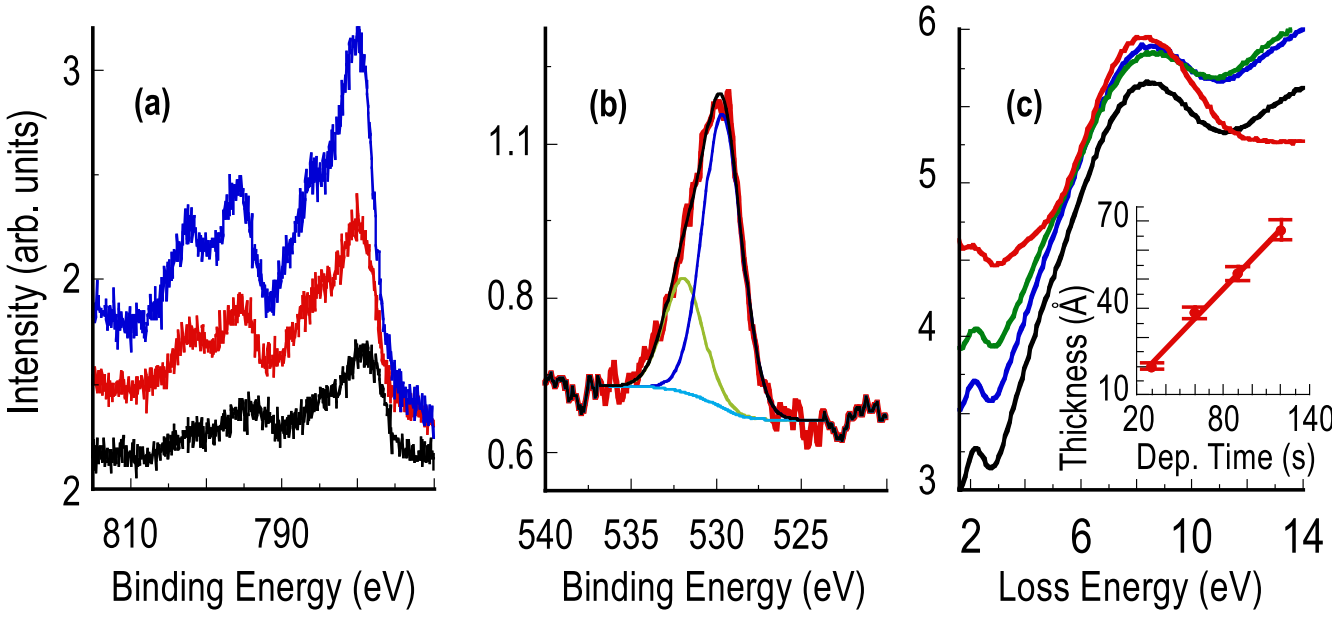

Figure 2. (a) Co 2p XPS spectra of CoO(111) films of varying thickness: 20 Å (black); 67 Å (red); 600 Å (blue). (b) Typical O 1s XPS spectrum of CoO(111) (shown here for a 67 Å film), decomposed into components for the oxide and (at higher binding energy) OH. (c) EELS spectra of CoO films of varying thickness: 20 Å (red); 38.5 Å (green); 52 Å (blue); 67 Å (black). The inset shows XPS-derived CoO (111) thickness as a function of deposition time at 500 K.

surface hydroxylation [23]; the (111) surfaces of polar oxides with the rock salt structure, such as CoO, are prone to reconstruction (at or near room temperature), due to the unstable Madelung energy [13, 24]. Hydroxylation, however, reduces surface polarization, and can stabilize the (111) surface [24, 25].

EELS spectra acquired at a primary energy of 100 eV are shown in figure 2(c) and demonstrate that the EELS spectrum remains constant over a broad range of thicknesses. Results are presented for films of various thicknesses, ranging from 20 to 67 Å, and the transition that can be seen close to 2 eV is consistent with previous reports on CoO particles [26]. (The uniformity of our films is suggested by the inset to figure 2(c), demonstrating that rate increase in XPS-derived average film thickness with deposition time was approximately constant over the entire range of films studied.)

To summarize the results of this section, our LEED, XPS and EELS data (figures 1 and 2) are entirely consistent with the formation of a CoO(111) film at lower O_2 partial pressure. The chemical and electronic structure of the film remains constant over a broad range of film thicknesses. Reconstruction of this film is not observed, and this is attributable to the observed (figure 2(b)) surface hydroxylation.

3.2. Cobalt oxide growth at high O_2 partial pressure: Co_3O_4(111) on Ru (0001)

Turning to the properties of the films prepared at higher oxygen partial pressure (10^{-4} Torr), in figure 3 we show LEED spectra obtained in measurements of cobalt oxide films of average thickness 16.6 Å (panel (a)), 100 Å (panel (b)), and 280 Å (panel (c)). (Corresponding linescan profiles are displayed in figures 3(d)–(f).) The data of figure 3(b) reveal the presence of two six-fold patterns that are rotated by 30° with respect to each other. Similar rotated patterns have previously been reported for Co_3O_4(111) grown directly on Al_2O_3(0001), indicating twinning of the film [9, 10]. On the basis of this observation we conclude that the synthesized film is Co_3O_4. Analysis of the FWHM of the diffraction spots for the 280 Å film (figures 3(b) and (d)) indicates the presence of a domain size of 13.5 (±3) nm. The LEED data show that the primary Co_3O_4(111) lattice is in azimuthal registry with that of the Ru(0001) substrate. The reciprocal-space unit cells for the Ru(0001) lattice and for the Co_3O_4(111) lattice (figures 3(a) and (d)) indicate an in-plane Co_3O_4(111) direct lattice constant (∼5.65 Å) that is slightly greater than twice the Ru(0001) lattice constant, and consistent with a reported value for Co_3O_4(111) of 5.7 Å [12]. As with CoO, the diffraction spot line profiles for Co_3O_4(111) films exhibit a narrowing spot FWHM, and consequently an increasing domain size, with increasing average film thickness (figure S2 and table S1).

As for the results of our other spectroscopic analyses, the evolution of the Co_3O_4 Co 2p and O 1s XPS data are displayed in figures 4(a) and (b), respectively, and the EELS data are shown in figure 4(c). The evolution of film thickness with coverage (figure 4(c), inset) is linear, as with CoO, indicating that an increase of O_2 partial pressure has not altered the linearity of film growth with deposition time. XPS Co 2p results are shown for various film thicknesses in figure 4(a); for an average thickness greater than around 20 Å, the Co 2p spectrum—with Co $2p_{3/2}$ and Co $2p_{1/2}$ features near 780 eV and 795 eV, respectively, and a satellite feature (figure 4(a), arrow) near 790 eV—is in close agreement with those reported previously for Co_3O_4(111) single crystals [1, 21, 22] and for nanocrystalline films [27]. Thinner (<∼20 Å) films, however, exhibit Co 2p spectra which resemble that of CoO

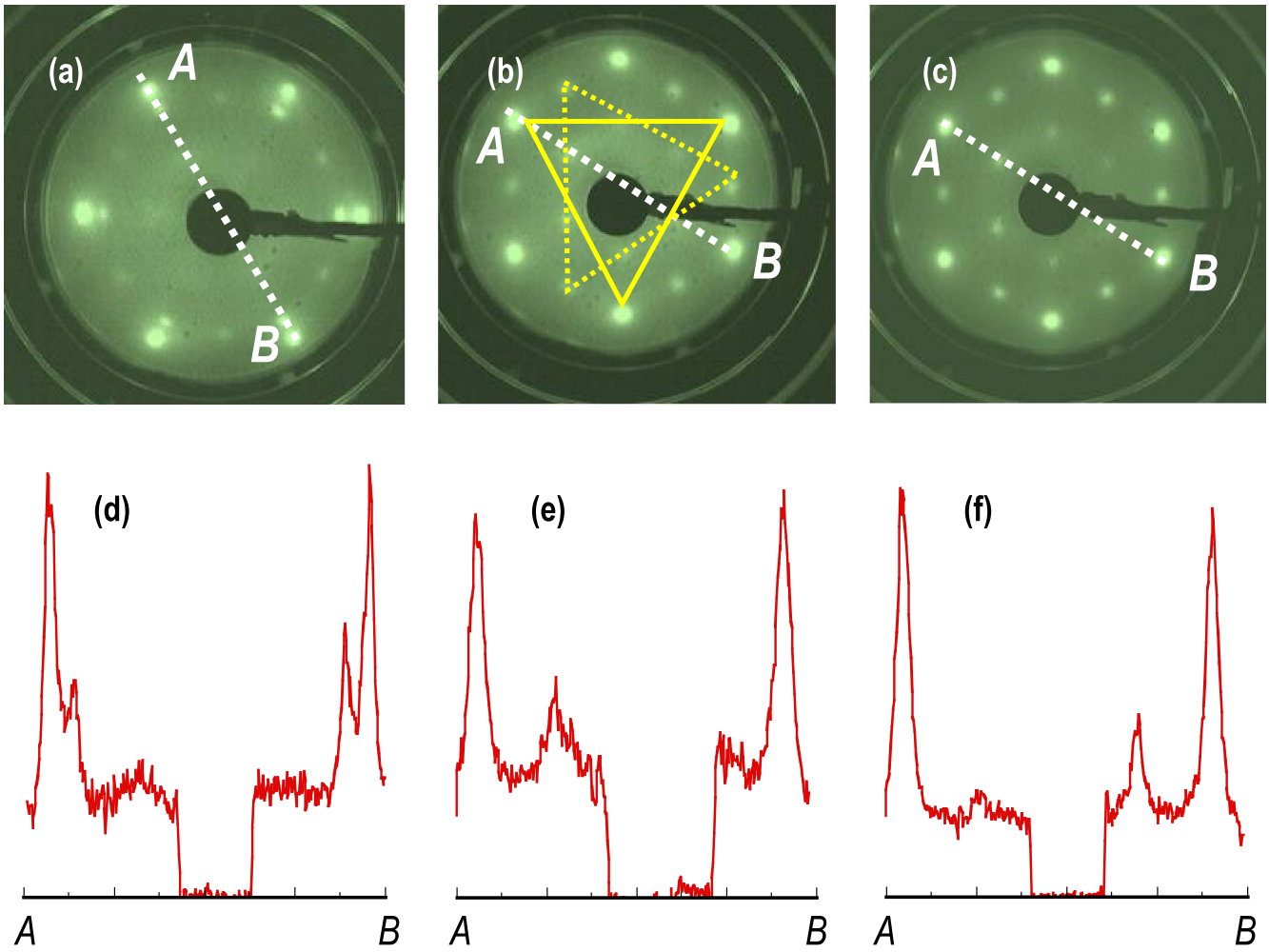

Figure 3. Evolution of LEED spectra in Co_3O_4(111) films of varying thickness: (a) 16.6 Å; (b) 100 Å; (c) 280 Å. Corresponding linescan profiles are shown in panels (d)–(f), respectively. The different oxide reciprocal lattices that are indicative of twinning are shown by the solid and dotted yellow triangles in panel (b). The LEED beam energy was 60 eV in all measurements.

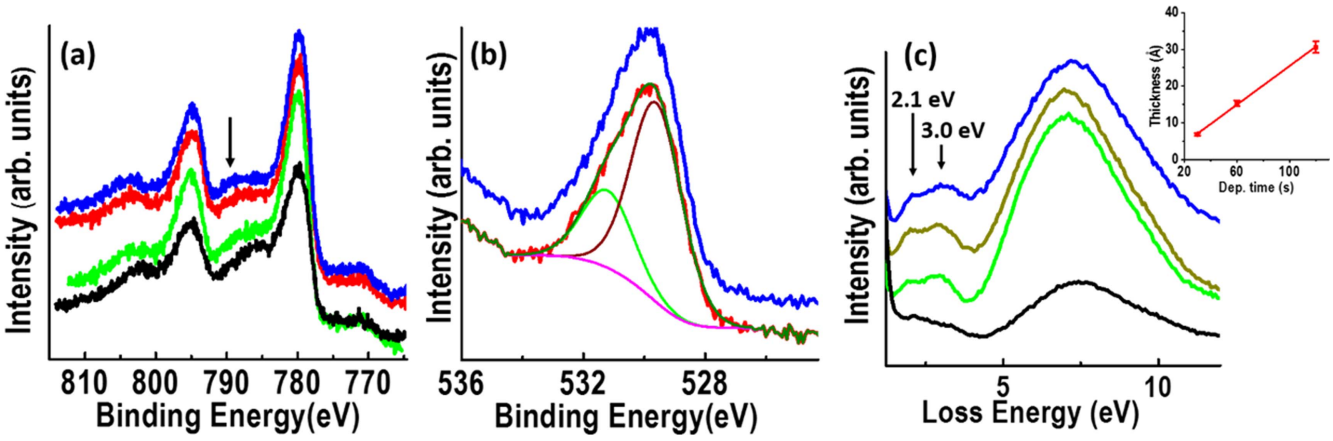

Figure 4. (a) Co 2p XPS spectra of Co_3O_4(111); 6.8 Å (black);); 22.9 Å (green); 100 Å (red); 280 Å (blue) thick film. Arrow marks the satellite feature. (b) O 1s XPS spectra; 100 Å (red with peak fit); 280 Å (blue) thick films.(c) EELS spectra of Co_3O_4 films of varying thickness: 6.8 Å (black); 22.9 Å (green); 30.65 Å (dark yellow); 280 Å (blue). Inset shows XPS-derived Co_3O_4 average film thickness as a function of deposition time at 500 K.

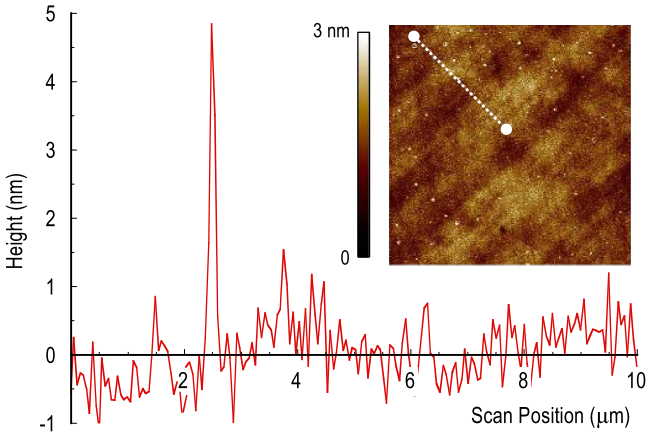

Figure 5. AFM imaging (inset) of the surface structure of a $Co_3O_4(111)/Ru(0001)$ film of 100 Å average oxide thickness, with corresponding line scan (main panel). The inset shows the topography variation measured over an area of 20 × 20 μm^2. The white dashed line indicates the path followed in the main panel.

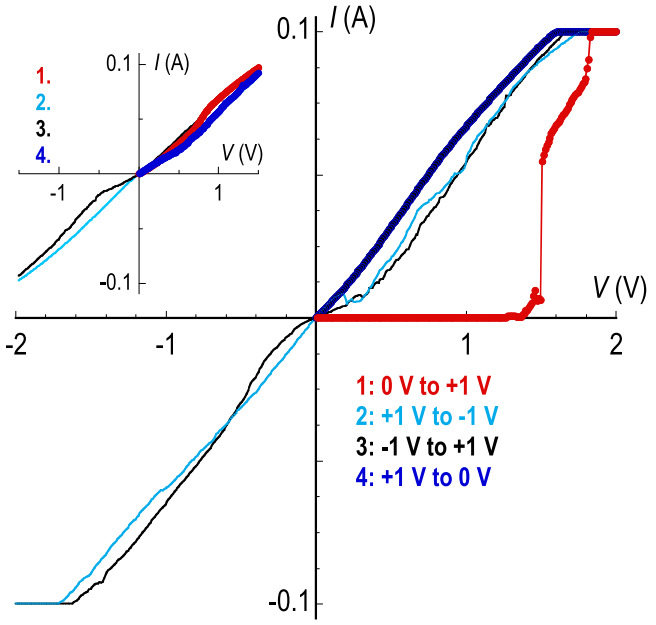

Figure 6. Dielectric breakdown in a 100 Å average thickness $Co_3O_4(111)$ film grown on Ru(0001). The sequence of the measurements is indicated in the lower-right quadrant. The inset represents the result of a second measurement, made at the same position on the film in order to check for reproducibility. The regions of saturated current in both the main panel and the inset correspond to conditions for which the current reached the pre-set compliance level of 100 mA.

(figure 2(a)) [1, 21, 22]. In contrast to the Co 2p spectra, the O 1s spectra (figure 4(b)) exhibit no significant change with film thickness, and indeed are very similar to those observed for CoO(111) films (see figure 2(b)). The main O 1s feature near a binding energy of 529 eV has been assigned to lattice O, while the broader feature at higher binding energy has been demonstrated, by comparison with vibrational spectra and H_2O exposure studies, to be due to surface hydroxylation [1].

The EELS spectra of figure 4(c) show an evolution with film thickness that is similar to that observed for the Co 2p spectra (of figure 4(a)). At average film thicknesses less than ∼17 Å, a small single loss feature may be discerned near 2 eV, with a larger more intense peak present near 7 eV. In contrast, thicker films exhibit a dual loss feature at 2.1 and 3.0 eV, as well as the larger peak near 7 eV. The observation of two interband transitions at 2.1 and 3.0 eV is consistent with optical measurements on non-epitaxial Co_3O_4 films, which have been found to exhibit two main transitions whose energies vary with experimental conditions of deposition and film microstructure [28, 29]. The EELS data in figure 4(c) therefore corroborate those of the Co 2p XPS data, confirming an evolution of the cobalt-oxide film structure and composition with average film thickness. The increase of XPS-derived average film thickness with deposition time (figure 4(c), inset) is, as with the CoO films, roughly linear over the range of thicknesses examined, indicating the uniformity of the deposited films.

3.3. Surface morphology and electrical characterization of the cobalt oxide films

In this section, we discuss the results of our investigations of the surface morphology and the electrical breakdown characteristics of the synthesized films. As noted already, due to the demonstrated capacity of $Co_3O_4(111)$ to support subsequent MBE of graphene, in this section we focus on the issue of this characterization with respect to these particular films. We start by presenting the surface morphology of the $Co_3O_4(111)/Ru(0001)$ film in figure 5, which shows the result of a 20 × 20 μm^2 *ex situ* AFM scan. The figure indicates a general surface-roughness corrugation of less than 1 nm, along with irregular local features of considerable height, the latter of which are likely particulates absorbed during *ex situ* handling.

Figure 6 shows a representative current–voltage characteristic for a 100 Å thick $Co_3O_4(111)/Ru(0001)$ film. The data were obtained by placing one tip of the probe station on the Co_3O_4 surface and the other on the underlying Ru substrate. This measurement therefore probes the electrical breakdown of the film and leads to behavior exemplified by that displayed in figure 6. The main panel of this plot shows data collected in a set of (four) different voltage sweeps; in the first portion (1) of the measurement, the current remains essentially quenched (note the behavior shown in the inset) up to a voltage of ∼1.2 V, at which point a dramatic onset is observed. This breakdown occurs at a field exceeding 1 MV cm^{-1}, indicative of the high dielectric quality of the grown film. Following this sweep, the voltage is then cycled back and forth (2 and 3), before it is finally returned back to zero. In order to gain insight into the nature of the breakdown that is observed in the main panel, a second measurement was then immediately performed at the same position, with the voltage swept over the same range as in the first measurement. The results of the latter measurement are shown in the inset to the main panel and make the following point clear; the breakdown induced in the first measurement appears irreversible, with a much lower resistance being obtained in measurements made subsequent to the initial sequence. As

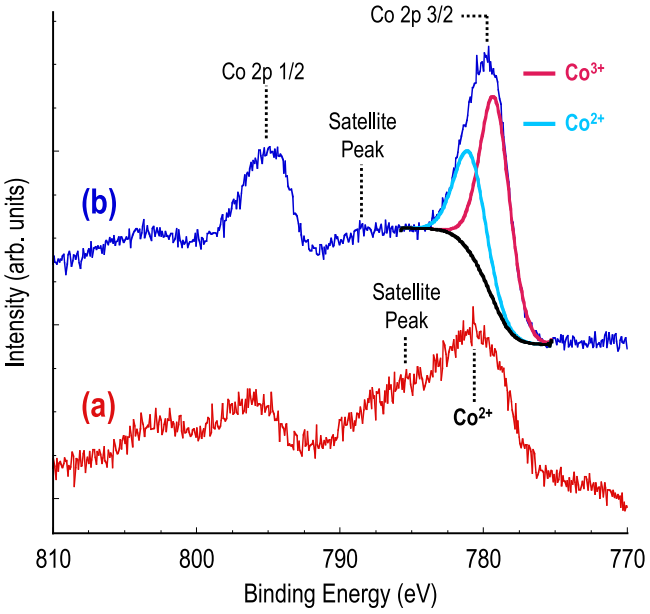

Figure 7. Co 2p XPS spectra of a (a) 67 Å thick CoO(111) film (b) 100 Å thick Co_3O_4(111) film. The Co $2p_{3/2}$ peak in (b) is decomposed into a Co^{+2} feature (light blue) and Co^{+3} feature (red) on a rising background (black).

such, this behavior is distinct from the memristor function that is often seen in resistive switching in cobalt oxides, and other transition metal oxides [30–32]. While the reasons for this difference require further study, we nonetheless note that the results of figure 6 establish the excellent dielectric strength of the oxide films.

4. Discussion

The data of figures 1 and 2 conclusively demonstrate that, for oxide film thicknesses exceeding 20 Å, films grown at an oxygen pressure of 7.5×10^{-7} Torr form CoO(111), while those of figures 4 and 5 establish that those grown at a higher oxygen pressure of 10^{-4} Torr form Co_3O_4(111). The LEED data for both oxide phases (figures 1 and 3) display relatively intense backgrounds compared to those of the clean Ru(0001) surface (figure 1(a)), and this may be indicative of a relatively high level of point defects (e.g., oxygen vacancies.) A similarly high background is observed for Co_3O_4(111) films grown on Al_2O_3(0001) [9], and for some, but not all Co_3O_4(111) films prepared on Ir(100) [2, 12]. The reasons for this high LEED background in some cases, but not others, and possible relevance to various applications, requires further study.

As we demonstrate in figure 7, the two different types of cobalt oxide film exhibit distinctive Co 2p spectra; the Co 2p spectrum of CoO(111) (curve (a) in figure 7) shows a broad Co $2p_{3/2}$ feature with a Co(II) peak at 780.1 eV, but broadened by a satellite feature, in excellent agreement with previous results [22, 23]. In contrast, the corresponding feature for Co_3O_4 (curve (b) in figure 7) exhibits a sharper Co(III) peak centered near 779.8 eV, and a Co(II) feature at slightly higher binding energy [22, 27].

A comparison of the data in figure 7 to the Co 2p XPS data in figure 4(a) indicates that Co_3O_4(111) film growth begins with the formation of a Co(II) oxide phase, and that no significant Co(III) is observed until the average oxide film thickness exceeds about 20 Å. The EELS data of figure 4(c) show a similar trend, and the LEED data of figure 3 indicate an absence of twinning for films thinner than 20 Å. A similar trend regarding twinning has been reported for the LEED images of Co_3O_4(111) films grown by O radical-assisted MBE directly on Al_2O_3(0001) [9], but the corresponding Co 2p XPS data in that case indicate the presence of Co(III) species on that substrate even at the earliest stages of film growth, with thicknesses much less than 20 Å. These data indicate different Co_3O_4 growth mechanisms on Ru(0001) compared to Al_2O_3(0001).

One possible explanation for the different trends found in the evolution of the Co 2p XPS spectra for Co_3O_4 film growth on ruthenium, as compared to alumina, is that, as Co(III) films occupy octahedral sites in the oxide [7], these sites may not be plentiful for oxide growth on Ru at average film thicknesses below 20 Å. Indeed, similar behavior has been reported [33] for FeO(111) and Fe_3O_4(111) growth on Ru(0001), where the minimum thickness of Fe_3O_4(111) islands was also estimated to be around 20 Å. In contrast, the formation of an initial Co_2O_3 phase has been proposed for Co_3O_4(111) growth on Al_2O_3(0001) [9].

The complex LEED pattern observed for thicker Co_3O_4(111) films grown on Ru(0001), consisting of two six-fold patterns rotated by 30^0 from each other (see figures 3(b) and (c)), is similar to those reported for Co_3O_4(111) grown by various methods on Ir [2, 12] and on Al_2O_3(0001) [9, 10, 34], and for Fe_3O_4(111) on Pt(111) or Ru(0001) [35]. This behavior is indicative of twinning [9, 10, 33], and appears to be a general phenomenon for both Co_3O_4(111) and Fe_3O_4(111), regardless of the specific substrate used or the growth method. The twinning itself has been attributed to two possible stacking sequences for the O^{2-} layers in the spinel phase, and has been discussed in detail for Co_3O_4(111) growth on Al_2O_3(0001) [34].

Both the CoO and Co_3O_4 films could be heated to at least 900 K in UHV without any detectable change in XPS, LEED or EELS spectra. Such thermal stability is unusual, as polar oxide surfaces, including CoO(111) (rocksalt structure) [12, 24] and also Co_3O_4(111) [12], are known to reconstruct at even moderate temperatures in UHV. It is also known, however, that these surfaces can be stabilized by hydroxylation [24, 25]. The XPS O 1s spectra of figures 2(b) and 4(b) indicate the presence of such surface hydroxylation for both of the oxide phases that we have synthesized. Similar hydroxylation has also been reported for both CoO(111) [23] and Co_3O_4(111) [1] surfaces prepared under UHV conditions. Since DFT calculations [7] indicate that the surface region of the relaxed unhydroxylated Co_3O_4(111) film is entirely composed of Co^{+2} cations, the distinctive XPS Co 2p spectra of figures 2(a) and 4(a), as well as the surface-sensitive EELS spectra of figures 2(c) and 4(c), indicate that both films are

essentially unreconstructed and bulk-terminated under these conditions due to surface hydroxylation.

The suitability of the synthesized $Co_3O_4(111)$ films for device applications is suggested by the AFM measurements of figure 5, and by the electrical-resistivity data of figure 6. The large-area AFM data indicate that the typical surface roughness is around a nanometer or less, certainly suitable for subsequent thin-film growth. A dielectric breakdown strength in excess of 1 MV cm^{-1} (figure 6) is extremely promising for a variety of low-voltage applications. The ability, however, to support direct graphene growth [7, 8, 36], and possibly the growth of other 2D materials, on $Co_3O_4(111)$, broadens potential device applications.

5. Conclusions

The data presented here demonstrate that Co MBE, performed on a $Ru(0001)/Al_2O_3(0001)$ substrate at 500 K and under UHV conditions, yields CoO(111) at a background O_2 pressure of 7.5×10^{-7} Torr, and $Co_3O_4(111)$ under identical growth conditions except for a background pressure of 10^{-4} Torr. $Co_3O_4(111)$ formation, including the observation of twinning (LEED), the presence of Co(III) in the Co 2p XPS spectrum, and characteristic EELS spectra, are only observed under such growth conditions for films with average thickness above 20 Å. Both oxide phases are hydroxylated under these deposition conditions, and show no evidence of reconstruction. They are also stable upon annealing to 900 K in UHV, without observable changes in their XPS, LEED or EELS spectra. The $Co_3O_4(111)$ film has an AFM-determined average surface roughness of less than a nanometer, and a dielectric breakdown voltage in excess of 1 MV cm^{-1}. $Co_3O_4(111)$ films are therefore suitable for a variety of device applications, including in potential graphene spintronic devices.

Acknowledgments

Work at UNT was supported by was supported by the NSF under grant no. ECCS-1508991, and in part by C-SPIN, a funded center of STARnet, a Semiconductor Research Corporation (SRC) program sponsored by MARCO and DARPA under task IDs 2381.001 and 2381.006. Work at Buffalo was supported by the NSF under grant. No. ECCS-1509221. Work at UNL was supported by the NSF under grant No. ECCS-1508541. Work at Caltech was supported was supported by the NSF (DMR-1436985) and DOE (DE-SC0014607).

ORCID iDs

Jeffry A Kelber https://orcid.org/0000-0002-3259-9068
Peter A Dowben https://orcid.org/0000-0002-2198-4710

References

[1] Petitto S C, Marsh E M, Carson G A and Langell M A 2008 Cobalt oxide surface chemistry: the interaction of CoO(100), $Co_3O_4(110)$ and $Co_3O_4(111)$ with oxygen and water *J. Mol. Cat.* A **281** 49–58
[2] Ferstl P *et al* 2015 Adsorption and activation of CO on $Co_3O_4(111)$ thin films *J. Phys. Chem.* C **119** 16688–99
[3] Meher S K and Rao G R 2011 Ultralayered Co_3O_4 for high-performance supercapacitor applications *J. Phys. Chem.* C **115** 15646–54
[4] Chen J and Selloni A 2012 Electronic states and magnetic structure at the $Co_3O_4(110)$ surface: a first-principles study *Phys. Rev.* B **85** 085306
[5] Chen J, Wu X and Selloni A 2011 Electronic structure and bonding properties of cobalt oxide in the spinel structure *Phys. Rev.* B **83** 245204
[6] Wu N and Dowben P A 2011 Magnetic surface states in high polarization materials *Proc. SPIE* **8100** 8100T
[7] Beatty J, Cheng T, Cao Y, Driver M S, Goddard W A III and Kelber J A 2017 Nucleation of graphene layers on magnetic oxides: $Co_3O_4(111)$ and $Cr_2O_3(0001)$ from theory and experiment *J. Phys. Chem. Lett.* **8** 188–92
[8] Wang Y, Kong L, Pasquale F L, Cao Y, Dong B, Tanabe I, Binek C, Dowben P A and Kelber J A 2013 Graphene mediated domain formation in exchange coupled graphene/$Co_3O_4(111)$/Co(0001) trilayers *J. Phys.: Condens. Matter* **25** 472203
[9] Vaz C A F, Prabhkaran D, Altman E I and Henrich V E 2009 Experimental study of the interfacial cobalt oxide in Co_3O_4/alpha-$Al_2O_3(0001)$ epitaxial films *Phys. Rev.* B **80** 155457
[10] Vaz C A F, Heinrich V E, Ahn C H and Altman E I 2009 Growth and characterization of thin epitaxial $Co_3O_4(111)$ films *J. Crystal Growth* **311** 2648–54
[11] Heinz K and Hammer L 2013 Epitaxial cobalt oxide films on Ir(100)—the importance of crystallographic analyses *J. Phys.: Condens. Matter* **25** 173001
[12] Meyer W, Biedermann K, Gubo M, Hammer L and Heinz K 2008 Surface structure of polar $Co_3O_4(111)$ films grown epitaxially on Ir(100)-(1 × 1) *J. Phys.: Condens. Matter* **20** 265011
[13] Biedermann K, Gubo M, Hammer L and Heinz K 2009 Phases and phase transitions of hexagonal cobalt oxide films on Ir(100)-(1 × 1) *J. Phys.: Condens. Matter* **21** 185003
[14] Zheng M, Willey M and West A C 2005 Electrochemical nucleation of copper on ruthenium *Electrochem. Solid State Lett.* **8** C151–4
[15] Sutter P W, Flege J and Sutter E A 2008 Epitaxial graphene on ruthenium *Nat. Mater.* **7** 406–11
[16] Van Staden M J and Roux J P 1990 The superposition of carbon and ruthenium Auger spectra *Appl. Surf. Sci.* **44** 259–62
[17] Seah M P 1990 Quantification of AES and XPS *Practical Surface Analysis, Volume 1—Auger and X-ray Photoelectron Spectroscopy* ed D Briggs and M P Seah 2nd edn (New York: Wiley) pp 201–55
[18] Powell C J and Jablonski A 2003 NIST Electron Effective Attenuation Lengths Database, version 1.1 www.NIST.gov
[19] Tanuma S, Powell C J and Penn D R 2003 Calculation of electron inelastic mean free paths (IMFPS): VII. Reliability of the TPP-2M predictive equation *Surf. Interface Anal.* **35** 268–75
[20] van Hove M A, Weinberg W H and Chan C-M 1986 *Low-Energy Electron Diffraction Experiment, Theory and Surface Structure Determination* (*Springer Series in Surface Sciences*) ed G Ertl and R Gomer (New York: Springer) pp 48–90

[21] Petito S C and Langell M A 2004 Surface composition and structure of Co_3O_4(110) and the effect of impurity segregation *J. Vac. Sci. Technol.* A **22** 1690–5
[22] Langell M A, Anderson M D, Carson G A, Peng L and Smith S 1999 Valence-band electronic structure of Co_3O_4 epitaxy on CoO(100) *Phys. Rev.* B **59** 4791–5
[23] Hassel M and Freund H-J 1995 NO on CoO(111)/Co(0001): hydroxyl-assisted adsorption *Surf. Sci.* **325** 163–8
[24] Cappus D, Xu C, Ehrlich D, Dillmann B, Ventrice C A Jr, Al Shamery K, Kuhlenbeck H and Freund H 1993 Hydroxyl groups on oxide surfaces: NiO(100), NiO(111), and Cr_2O_3(111) *Chem. Phys.* **177** 533–46
[25] Lazarov V K, Plass R, Poon H, Saldin D K, Weinert M, Chambers S A and Gajdardziska-Josifovska M 2005 Structure of the hydrogen-stabilized MgO(111)-(1 × 1) polar surface: integrated experimental and theoretical studies *Phys. Rev.* B **71** 115434
[26] Hagelin-Weaver H A E, Hoflund G B, Minahan D M and Salaita G N 2004 Electron energy loss investigation of Co metal, CoO and Co_3O_4 before and after Ar bombardment *Appl. Surf. Sci.* **235** 420–8
[27] Berenguer R T, Fuertes A B, Quijada C and Morallon E 2008 Cyanide and phenol oxidation on nanostructured Co_3O_4 electrodes prepared by different methods *J. Electrochem. Soc.* **155** K110–5
[28] Patil P S, Kadam L D and Lokhande C D 1996 Preparation and characterization of spray pyrolysed cobalt oxide thin films *Thin Solid Films* **272** 29–32
[29] Barakat N A M, Khil M S, Sheikh F A and Kim H Y 2008 Synthesis and optical properties of two cobalt oxides (CoO and Co_3O_4) nanofibers produced by electrospinning process *J. Phys. Chem.* C **113** 12225–33
[30] Hu W, Qin N, Wu G, Lin Y, Li S and Bao D 2012 Opportunity of spinel ferrite materials in nonvolatile memory device applications based on their resistive switching performances *J. Am. Chem. Soc.* **134** 14658–61
[31] Nagashima K, Yanagida T, Oka K, Taniguchi M, Kawai T, Kim J and Park B H 2010 Resistive switching multistate nonvolatile memory effects in a single cobalt oxide nanowire *Nano Lett.* **20** 1359–63
[32] Sawa A 2008 Resistive switching in transition metal oxides *Mater. Today* **11** 28–36
[33] Ketteler G and Ranke W 2003 Heteroepitaxial growth and nucleation of iron oxide films on Ru(0001) *J. Phys. Chem.* B 2003 **107** 4320–33
[34] Bursik J M, Kuzel R and Mika F 2015 Growth and characterization of thin oriented Co_3O_4(111) films obtained by decomposition of layered cobaltates Na_xCoO_2 *J. Solid State Chem.* **227** 17–24
[35] Lewandowski M, Groot I M N, Qin Z, Ossowski T, Pabisiak T, Kiejna A, Pavlovska A, Shaikhutdinov S, Freund H and Bauer E 2016 Nanoscale patterns on polar oxide surfaces *Chem. Mater.* **28** 7433–43
[36] Zhou M, Pasquale F L, Dowben P A, Boosalis A, Schubert M, Darakchieva V, Yakimova R and Kelber J A 2012 Direct graphene growth on Co_3O_4(111) by molecular beam epitaxy *J. Phys.: Condens. Matter* **24** 072201